A KINETIC DISCONTINUOUS GALERKIN METHOD FOR THE NONCONSERVATIVE BITEMPERATURE EULER MODEL *

DENISE AREGBA-DRIOLLET †, AFAF BOUHARGUANE ‡, AND STÉPHANE BRULL §

Abstract. This paper is devoted to the construction of a discontinuous Galerkin (DG) discretisation for the nonconservative bitemperature Euler system *via* a discrete BGK formulation. This formulation is compatible with the entropy properties of the system and thus provides admissible solutions. The DG method is used to approximate the linear transport part of the BGK model while the force and source-terms are treated implicitly but with explicit expressions. High order in time has also been investigated using SSP Runge-Kutta methods. We numerically show the good agreement of our results with the ones provided by other schemes, including solutions with shocks.

Keywords. nonconservative hyperbolic system, discrete BGK approximation, discontinuous Galerkin methods, Runge-Kutta methods.

AMS subject classifications. 65M08, 35L60, 76X05, 35Q31

1. Introduction

This paper is devoted to the approximation of the bitemperature Euler system from a Discontinuous Galerkin (DG hereafter) method applied to a kinetic formulation proposed in [5] and that is based on a discrete BGK model. The present fluid model is able to treat out of equilibrium regimes. The standard strategy in plasma physics for simulating such regimes is to develop PIC methods, that directly solve the kinetic equations. But these methods are computationally very expensive. Therefore, the bitemperature model is a compromise between the precision of the kinetic models and the lower numerical cost of fluid models. This system is made of two conservation equations for mass and momentum and of two nonconservative equations for ionic and electronic energies. It describes the interaction of a mixture of thermalized ions and electrons in a quasi-neutral regime. This system is nonconservative because of the presence of a relaxation source term and of products between velocity and pressure gradients. Those products make difficult the definition of weak solutions. In [21], a general framework has been developed in order to define shocks in this context by using families of paths. The generalization of this approach to a numerical setting has been considered in [28]. However, even if the path is known theoretically, the numerical determination of the path is delicate [2]. It is shown in [9] that the entropy does not provide a symmetrizer for this system. However, a symmetrizer can be computed. In [20], the authors consider the bitemperature Euler system with diffusive terms and by assuming that the electrons are isentropic. In that case, the system is transformed into a system of conservation laws. This approach has also been used in [30] where magnetic fields are considered and a conservation equation on electronic entropy is derived. In [14], magnetic fields are also considered in a transverse magnetic configuration. Moreover, a Suliciu scheme is derived and proved to be entropic. In [31], the authors perform a Chapman-Enskog expansion by introducing a small parameter representing the ratio

*Submitted to the editors DATE.

†Univ. Bordeaux, CNRS, Bordeaux INP, IMB, UMR 5251, F-33400 Talence, France (denise.aregba@math.u-bordeaux.fr).

‡Univ. Bordeaux, CNRS, Bordeaux INP, IMB, UMR 5251, F-33400 Talence, France INRIA Bordeaux Sud-Ouest, MEMPHIS team, (afaf.bouharguane@math.u-bordeaux.fr) .

§Univ. Bordeaux, CNRS, Bordeaux INP, IMB, UMR 5251, F-33400 Talence, France (stephane.brull@math.u-bordeaux.fr).

between electronic and ionic molecular masses. At the end, they obtain a system with an hyperbolic part for ions and a parabolic part for electrons.

In the context of kinetic equations, a DG method can be used to discretize the space variable, whereas the velocity variable is treated by using a DVM discretization. In ([25], [26], [12]), the authors couple a DG discretization in the space variable with a spectral method in the velocity variable for the Boltzmann equation. However in the present paper, the aim is different, because our goal is to solve the bitemperature Euler system. Hence, we perform a kinetic reformulation of the problem and next we apply a DG discretization. The final algorithm is obtained by using a transport projection procedure.

Discrete BGK schemes for general hyperbolic systems of conservation laws have been introduced in [11, 27]. The method is performed by a transport projection approach. The advantage is to put the nonlinearity inside the relaxation term whereas the transport term is linear with constant advection velocities. The bitemperature model under consideration is obtained in [5] by using an hydrodynamic limit starting from a BGK model coupled with Poisson and Ampère equations in a quasi-neutral regime. In particular, it is shown that the nonconservative terms come from the Ohm's law defining the electric field. By using this asymptotic a finite volume BGK scheme generalizing the Aregba-Natalini method [11] to a nonconservative setting has been designed in [5]. In particular, a force term is incorporated in the discrete BGK formulation in order to deal with the nonconservative terms. This formulation leads to the resolution of an hyberbolic system from a BGK relaxation process. Hence we have to deal with a linear advection term and a source term. Moreover, a Suliciu approach also is developed in [5] by relaxing on the pressures and several comparisons are performed with different schemes. Next, in [7] the kinetic approach has been generalized to a polyatomic setting by using a kinetic model with a continuous energy variable. In [15], the authors use the asymptotic from the BGK model toward the bitemperature Euler system considered in [5]. Next they derive an asymptotic preserving scheme for this limit with a DVM discretization for the velocity variable. The bi-dimensional case has been considered in [10] and a second order finite volume scheme has been obtained. In [6], a Navier-Stokes system has been derived from a Chapman-Enskog expansion and by computing viscous terms, generalizing the model considered in [17]. However, as far as we know, there is no work on the implementation of high order methods for the nonconservative bitemperature model.

Recent works use the discrete BGK setting with various approximation methods in the conservative case. In [3, 4], the authors perform a RD scheme for the compressible Euler system in the space variable. The time discretization is obtained by using a DeC method [1]. In [19] the authors constructed a high-order implicit palindromic discontinuous Galerkin method from kinetic-relaxation approximation for solving general hyperbolic systems of conservation laws. In [22], this approach is used to solve Maxwell's equations. The aim of the present work is to provide high order methods for the nonconservative bitemperature Euler system which use a DG scheme on the discrete BGK formulation with k-th degree basis for the spacial discretization and with an order $(k+1)$-SSP-Runge-Kutta method for the time integration.

This paper is organised as follows. Section 2 introduces the bitemperature Euler system. Section 3 deals with the presentation of the discrete BGK models in the conservative and in the nonconservative case. In particular the obtention of the bitemperature

model from the kinetic formulation developed in [5] is explained. In section 4, the DG method applied to the discrete BGK approximation is described. In particular, the order in time is increased in order to be consistent with the order in the space variable. Section 5 is devoted to numerical experiments. We investigate the accuracy of the proposed schemes on some examples. We also compare our methods with other existing numerical schemes. An important result in this nonconservative framework is that they converge to the same solutions, even in the presence of shocks.

2. Bitemperature Euler system Subscripts e and i respectively denote electronic and ionic quantities. We denote by ρ_e and ρ_i the electronic and ionic densities, $\rho=\rho_e+\rho_i$ the total density, m_e and m_i the related masses, c_e and c_i the mass fractions. These variables satisfy

$$\rho_e=m_e n_e=c_e\rho,\quad \rho_i=m_i n_i=c_i\rho,\quad m_e>0,\quad m_i>0,\quad c_e+c_i=1. \tag{2.1}$$

Quasineutrality is assumed, so that the ionization ratio $Z=n_e/n_i$ is a constant. This implies that the electronic and ionic mass fractions are constant and given by

$$c_e=\frac{Zm_e}{m_i+Zm_e},\quad c_i=\frac{m_i}{m_i+Zm_e}. \tag{2.2}$$

Electronic and ionic velocities u_e,u_i are assumed to be in equilibrium in the model. Hence, $u_e=u_i=u$, where u denotes mixture velocity. The pressure of each species satisfies a gamma-law with its own γ exponent :

$$p_e=(\gamma_e-1)\rho_e\varepsilon_e=n_e k_B T_e,\quad p_i=(\gamma_i-1)\rho_i\varepsilon_i=n_i k_B T_i,\quad \gamma_e>1,\quad \gamma_i>1, \tag{2.3}$$

where k_B is the Boltzmann constant ($k_B>0$), ε_α and T_α represent respectively the internal specific energy and the temperature of species α for $\alpha=e,i$.

Denoting by $|\cdot|$ the euclidean norm in $\mathbb{R}^D$, the total energies for the particles are defined by

$$\mathcal{E}_\alpha=\rho_\alpha\varepsilon_\alpha+\frac{1}{2}\rho_\alpha|u|^2,\quad \alpha=e,i. \tag{2.4}$$

We denote by $\nu_{ei}\geq 0$ the interaction coefficient between the electronic and ionic temperatures. The model consists of two conservative equations for mass and momentum and two nonconservative equations for the energies:

$$\begin{cases}\partial_t\rho+\operatorname{div}(\rho u)=0,\\ \partial_t(\rho u)+\operatorname{div}(\rho u\otimes u+(p_e+p_i)\mathrm{I})=0,\\ \partial_t\mathcal{E}_e+\operatorname{div}(u(\mathcal{E}_e+p_e))-u\cdot\nabla(c_i p_e-c_e p_i)=\nu_{ei}(T_i-T_e),\\ \partial_t\mathcal{E}_i+\operatorname{div}(u(\mathcal{E}_i+p_i))+u\cdot\nabla(c_i p_e-c_e p_i)=-\nu_{ei}(T_i-T_e),\end{cases} \tag{2.5}$$

where I represents the identity matrix in $\mathbb{R}^3$. In the following we denote

$$\mathcal{U}=(\rho,\rho u,\mathcal{E}_e,\mathcal{E}_i),\quad U_\alpha=(\rho_\alpha,\rho_\alpha u,\mathcal{E}_\alpha). \tag{2.6}$$

The system (2.5) is hyperbolic, diagonalisable and owns 3 eigenvalues λ_-, λ_0 (with multiplicity $D+1$ where D is the space dimension), λ_+: for any $\omega\in S^{D-1}$

$$\lambda_-=u\cdot\omega-a,\qquad \lambda_0=u\cdot\omega,\qquad \lambda_+=u\cdot\omega+a$$

where

$$a=\sqrt{\sum_{\alpha=e,i}\frac{\gamma_\alpha p_\alpha}{\rho}} \tag{2.7}$$

is the sound velocity. The fields related to $\lambda_\pm$ are genuinely nonlinear, while the field related to λ_0 is linearly degenerate.

Defining the total energy $\mathcal{E}=\mathcal{E}_e+\mathcal{E}_i$ and the total pressure $p=p_e+p_i$, one can note that if $\mathcal{U}$ is a solution of system (2.5) then $(\rho,\rho u,\mathcal{E})$ satisfies the following conservative system:

$$\begin{cases}\partial_t\rho+\operatorname{div}(\rho u)=0,\\ \partial_t(\rho u)+\operatorname{div}(\rho u\otimes u+p\mathrm{I})=0,\\ \partial_t\mathcal{E}+\operatorname{div}(u(\mathcal{E}+p))=0.\end{cases} \tag{2.8}$$

If $\gamma_e=\gamma_i$ this is the wellknown monotemperature Euler system. But even in this case, one has to deal with one more equation to determine electronic and ionic temperatures. If $\gamma_e\neq\gamma_i$ system (2.8) is not closed. We want to underline the fact that in both cases, the solutions of system (2.5) are to be defined in the context of nonconservative equations were the product of a possibly discontinuous function with a Dirac measure appears. To give a sense to such solutions, one has to bring more physical information. In [5] we obtained solutions of (2.5) as hydrodynamic limits of solutions of an underlying, physically realistic BGK model. The entropy-entropy flux of species α is defined as

$$\eta_\alpha(U_\alpha)=-\frac{\rho_\alpha}{m_\alpha(\gamma_\alpha-1)}\left[\ln\left(\frac{(\gamma_\alpha-1)\rho_\alpha\varepsilon_\alpha}{(\rho_\alpha)^{\gamma_\alpha}}\right)+C\right],\quad Q_\alpha(U_\alpha)=\eta_\alpha(U_\alpha)u. \tag{2.9}$$

For $\mathcal{U}=(\rho,\rho u,\mathcal{E}_e,\mathcal{E}_i)$, one sets $U_\alpha=(c_\alpha\rho,c_\alpha\rho u,\mathcal{E}_\alpha)$. The total entropy-entropy flux pair for (2.5) is

$$\eta(\mathcal{U})=\eta_e(U_e)+\eta_i(U_i),\qquad Q(\mathcal{U})=\eta(\mathcal{U})u. \tag{2.10}$$

We proved the following entropy inequality for these hydrodynamic limits:

$$\partial_t\eta(\mathcal{U})+\operatorname{div}Q(\mathcal{U})\leq-\frac{\nu_{ei}}{k_BT_iT_e}(T_i-T_e)^2. \tag{2.11}$$

We then defined an admissible solution of (2.5) as a solution satisfying this inequality.

In the following we consider the 1D version of system (2.5):

$$\begin{cases}\partial_t\rho+\partial_x(\rho u)=0,\\ \partial_t(\rho u)+\partial_x(\rho u^2+p_e+p_i)=0,\\ \partial_t\mathcal{E}_e+\partial_x(u(\mathcal{E}_e+p_e))-u\partial_x(c_ip_e-c_ep_i)=\nu_{ei}(T_i-T_e),\\ \partial_t\mathcal{E}_i+\partial_x(u(\mathcal{E}_i+p_i))+u\partial_x(c_ip_e-c_ep_i)=-\nu_{ei}(T_i-T_e).\end{cases} \tag{2.12}$$

3. BGK models This section is devoted to the presentation of discrete BGK models that have been introduced for system of conservation laws in [11] and then generalized to the nonconservative case in [5, 8, 10].

3.1. Underlying kinetic (BGK) models for the conservative compressible Euler system We start from BGK models for the Euler monotemperature equations. Denoting

$$U=(\rho,\rho u,\mathcal{E})\in\Omega\subset\mathbb{R}^3,\quad F(U)=(\rho u,\rho u^2+p,u(\mathcal{E}+p)),$$

the Euler system is a system of conservation laws:

$$\partial_t U+\partial_x F(U)=0. \tag{3.1}$$

We assume that $p=(\gamma-1)(\mathcal{E}-\frac{1}{2}\rho u^2)$. We follow the framework proposed by F. Bouchut in [13]. We define a measure space $(X,d\xi)$, a real valued function a defined on X, a "maxwellian function" M from $\mathbb{R}^3\times X$ onto $\mathbb{R}^p$, and a "moment operator" P from X to $\mathcal{L}(\mathbb{R}^p,\mathbb{R}^3)$ such that for all $U\in\Omega$:

$$\int_X P(\xi)(M(U,\xi))d\xi=U,\quad \int_X P(\xi)\,(a(\xi)M(U,\xi))\,d\xi=F(U). \tag{3.2}$$

Let $f^\varepsilon(x,t,\xi)\in\mathbb{R}^p$ be a solution of

$$\partial_t f^\varepsilon+a(\xi)\partial_x f^\varepsilon=\frac{1}{\varepsilon}(M(U(f^\varepsilon),\xi)-f^\varepsilon),$$

with

$$U(f^\varepsilon)(x,t)=\int_X P(\xi)(f^\varepsilon(x,t,\xi))d\xi.$$

Formally if $\lim_{\varepsilon\to 0}f^\varepsilon=f$, then $f(x,t,\xi)=M(U(f)(x,t),\xi)$ and $U(f)$ is a solution of (3.1). In [13], conditions are given for the existence of microscopic entropies compatible with all the entropies of the macroscopic limit.

3.1.1. Example 1: a physically realistic BGK model Here we set

$$X=\mathbb{R}^3,\quad \xi=v,\quad d\xi=dv,\quad a(\xi)=v_1,\quad p=1$$

and $M(U,v)\in\mathbb{R}$ is given by

$$M(U)=\frac{n}{(2\pi k_B T/m)^{3/2}}exp(-\frac{|v-u|^2}{2k_BT/m}). \tag{3.3}$$

The moment operator is defined as

$$P(\xi)(M)=(m,mv_1,\frac{m|v|^2}{2})M.$$

As $f^\varepsilon(x,t,v)\in\mathbb{R}$, it is a rank one model. This model is compatible with the physical entropy of Euler system. It corresponds to the classical BGK model in the context of rarefied gases. Moreover, the model (2.12) has been derived in [5] by using this formalism.

3.1.2. Example 2: a discrete velocity BGK model Here $X=\{1,2\}$, $a(\xi)=\lambda_\xi$ with $\lambda_2>\lambda_1$, $P(\xi)=I_d$, $p=3$ and

$$M(U,1)=\frac{\lambda_2 U-F(U)}{\lambda_2-\lambda_1},\quad M(U,2)=\frac{-\lambda_1 U+F(U)}{\lambda_2-\lambda_1}, \tag{3.4}$$

see [11]. For any Euler entropy, the existence of related microscopic entropies is ensured under Liu's subcharacteristic condition, see [13]:

$$\sigma(F'(U))\subset]\lambda_1,\lambda_2[.$$

The numerical scheme developed in the present paper is based on this model.

3.2. BGK models for the nonconservative bitemperature Euler equations

We take a BGK model for the monotemperature Euler system (3.1) with $\gamma=\gamma_e$ and $\gamma=\gamma_i$. We choose

$$X_e=X_i=X,\quad a_e(\xi)=a_i(\xi)=a(\xi),\quad P_e(\xi)=P_i(\xi)=P(\xi).$$

In the following, we recall the kinetic formulation of bitemperature system (2.12) that has been performed in [5]. For more details we refer to this paper. The authors consider a kinetic system which consists of a BGK model for gas mixtures coupled with the Ampère and Poisson equations through the electric force. The BGK model satisfies classical properties (H theorem, correct equilibrium states, ...). Next the authors consider a quasi-neutral regime where the collisions between the same species are dominant and perform an hydrodynamic limit leading to the system (2.12). Throughout this step, the electric field is shown to satisfies a generalized Ohm's law defining the nonconservative products. Next by using this asymptotic, a discrete BGK formulation in a nonconservative setting has been performed in [5]. The discrete BGK model is based on the formalism developed initially in [11]. The present model displayed in (3.5) is not devoted to have a physical meaning. But it is used to develop a numerical scheme for the fluid limit (2.12). In the following lines, we detail the asymptotic developed on the discrete BGK model of section 3.1.2.

The equations for f_e^ε and f_i^ε belonging to $\mathbb{R}^3$ are coupled with the ones for the electric field E:

$$\begin{cases}\partial_t f_e^\varepsilon + a(\xi)\partial_x f_e^\varepsilon + \dfrac{q_e}{m_e}E^\varepsilon \mathcal{N} f_e^\varepsilon = \dfrac{1}{\varepsilon}(M_e - f_e^\varepsilon) + B_{ei}(f_e^\varepsilon, f_i^\varepsilon),\\ \partial_t f_i^\varepsilon + a(\xi)\partial_x f_i^\varepsilon + \dfrac{q_i}{m_i}E^\varepsilon \mathcal{N} f_i^\varepsilon = \dfrac{1}{\varepsilon}(M_i - f_i^\varepsilon) + B_{ie}(f_i^\varepsilon, f_e^\varepsilon),\\ \partial_t E^\varepsilon = -\dfrac{1}{\varepsilon^2}\left(\dfrac{q_e}{m_e}\rho_e^\varepsilon u_e^\varepsilon + \dfrac{q_i}{m_i}\rho_i^\varepsilon u_i^\varepsilon\right),\\ \partial_x E^\varepsilon = \dfrac{1}{\varepsilon^2}\left(\dfrac{q_e}{m_e}\rho_e^\varepsilon + \dfrac{q_i}{m_i}\rho_i^\varepsilon\right).\end{cases} \tag{3.5}$$

The term $B_{\alpha\beta}$ represents the collisions between the different species α and β. The linear operator $\mathcal{N}f$ represents the force term ([5]) defined for $f(\xi)\in\mathbb{R}^3$ by

$$\mathcal{N}f(\xi) = \begin{pmatrix} 0 & 0 & 0\\ -1 & 0 & 0\\ 0 & -1 & 0\end{pmatrix}\begin{pmatrix} f_1(\xi)\\ f_2(\xi)\\ f_3(\xi)\end{pmatrix}.$$

In the classical case corresponding to subsection 3.1.1, this term is replaced by $E\cdot\nabla f$. For more precisions we refer to [5].

When ε tends to 0, we have formally

$$u_e=u_i=u,\quad \frac{q_e}{m_e}\rho_e+\frac{q_i}{m_i}\rho_i=0,\quad M_\alpha(U_\alpha)=f_\alpha. \tag{3.6}$$

Quasineutrality holds: $\rho=\rho c_e=\rho c_i$ and c_e, c_i are the constants defined in (2.2). The collision operator $B_{\alpha\beta}$ is computed when $f_\alpha=M_\alpha$ satisfying (3.6), so that

$$\int_X P(\xi)B_{\alpha\beta}(M_\alpha,M_\beta)d\xi = (0,0,\nu_{ei}(T_\beta-T_\alpha)).$$

The linear operator $\mathcal{N}$ ([5]) is such that

$$\int_X P(\xi)(\mathcal{N}M_\alpha(U_\alpha,\xi))d\xi = -(0,\rho_\alpha,\rho_\alpha u).$$

By taking the moments, it comes that

$$\begin{cases} \partial_t\rho_\alpha + \partial_x(\rho_\alpha u) = 0, & \alpha = e,i, \\ \partial_t(\rho_\alpha u) + \partial_x(\rho_\alpha u^2 + p_\alpha) - \dfrac{q_\alpha}{m_\alpha} E\rho_\alpha = 0, & \alpha = e,i, \\ \partial_t\mathcal{E}_e + \partial_x(u(\mathcal{E}_e + p_e)) - \dfrac{q_e}{m_e} E\rho_e u = \nu_{ei}(T_i - T_e), \\ \partial_t\mathcal{E}_i + \partial_x(u(\mathcal{E}_i + p_i)) - \dfrac{q_i}{m_i} E\rho_i u = -\nu_{ei}(T_i - T_e). \end{cases} \tag{3.7}$$

Considering

$$\begin{cases} \partial_t(\rho c_e u) + \partial_x(\rho c_e u^2 + p_e) - \dfrac{\rho_e q_e}{m_e} E = 0, \\ \partial_t(\rho c_i u) + \partial_x(\rho c_i u^2 + p_i) - \dfrac{\rho_i q_i}{m_i} E = 0 \end{cases}$$

leads to the expression of E ([5])

$$\frac{\rho_e q_e}{m_e} E = -\frac{\rho_i q_i}{m_i} E = c_i\partial_x p_e - c_e\partial_x p_i \tag{3.8}$$

and

$$\partial_t(\rho u) + \partial_x(\rho u^2 + p_e + p_i) = 0.$$

Hence replacing E by the expression (3.8) into (3.7), we get that $\mathcal{U} = (\rho, \rho u, \mathcal{E}_e, \mathcal{E}_i)$ is a solution of system (2.12). The relation (3.8) corresponds to a genaralized Ohm's law.

THEOREM 3.1. *Suppose that there exist microscopic entropies for the kinetic model (3.5) related to the entropy η. Let $\mathcal{U}$ be a solution of the Euler bitemperature model (2.12) obtained by passing to the limit in (3.5). Then one has the entropy inequality*

$$\partial_t\eta(\mathcal{U}) + \partial_x Q(\mathcal{U}) \le -\frac{\nu_{ei}}{k_B T_i T_e}(T_i - T_e)^2.$$

We define such a solution $\mathcal{U}$ as an admissible solution.

In the case of examples 1 and 2 above, the microscopic entropies exist, see [5] for details.

4. A Discontinuous Galerkin (DG) scheme This section is devoted to the discretisation of system (2.12) by using the discrete BGK model developed in section 3. We denote Δx and Δt the space and time steps and we mesh the real line by cells $C_K = [x_{K-\frac{1}{2}}, x_{K+\frac{1}{2}}]$ with $x_{K+\frac{1}{2}} - x_{K-\frac{1}{2}} = \Delta x$. In practice an interval is considered with appropriate boundary conditions : $K \in \{1,\dots,N\}$. We also denote by P^k the space of all polynomials of degree at most k.

4.1. Preliminary Let us consider a transport equation

$$\partial_t f + v\partial_x f = 0 \tag{4.1}$$

where $v \in \mathbb{R}$ and $f(x,t,v) \in \mathbb{R}$. We look for an approximation of $f(\cdot,t,v)$ under the form $\sum_{K=1}^{N} f^K(\cdot,t,v)$ where each $f^K(\cdot,t,v)$ has C_K as support and its restriction to C_K is in P^k. Let $\{\Phi_j^K, j=0,\dots,k\}$ be a basis of polynomial functions defined on C_K. For the numerical simulations given in Section 5, we used Lagrange polynomials as a local basis of P^k on C_K and below we denote $x_0^K,\dots,x_k^K$ the related Lagrange points. Outside C_K, $\Phi_j^K = 0$.

On C_K the approximate variational form of equation (4.1) is

$$\int_{C_K} \partial_t f^K(x,t,v)\Phi_i^K(x)dx - v\int_{C_K} f^K(x,t,v)(\Phi_i^K)'(x)dx \\ + v\hat{f}_{K+\frac{1}{2}}\Phi_i^K(x_{K+\frac{1}{2}}) - v\hat{f}_{K-\frac{1}{2}}\Phi_i^K(x_{K-\frac{1}{2}}) = 0, \quad i=0,\dots,k.$$

We have to choose a flux $v\hat{f}_{K+\frac{1}{2}} = h(f(x^-_{K+\frac{1}{2}}), f(x^+_{K+\frac{1}{2}}), v)$. We can set the following

$$h(f,g,v) = v\left(\frac{\lambda_2}{\lambda_2-\lambda_1}f - \frac{\lambda_1}{\lambda_2-\lambda_1}g\right) + \frac{\lambda_1\lambda_2}{\lambda_2-\lambda_1}(g-f) \tag{4.2}$$

where $\lambda_1 \le 0 \le \lambda_2$.

Another choice is the upwind flux: denoting $v^+ = \max(v,0)$, $v^- = \max(-v,0)$

$$h(f,g,v) = v^+ f - v^- g. \tag{4.3}$$

Now we write $f^K(x,t,v)$ as

$$f^K(x,t,v) = \sum_{j=0}^{k} f_j^K(t,v)\Phi_j^K(x). \tag{4.4}$$

We obtain

$$\sum_{j=0}^{k} M_{ij}^K \partial_t f_j^K(t,v) - v\sum_{j=0}^{k} S_{ij}^K f_j^K(t,v) + v\hat{f}_{K+\frac{1}{2}}\Phi_i^K(x_{K+\frac{1}{2}}) - v\hat{f}_{K-\frac{1}{2}}\Phi_i^K(x_{K-\frac{1}{2}}) = 0$$

where we have defined two matrices M^K and S^K:

$$M_{ij}^K = \int_{C_K} \Phi_j^K \Phi_i^K dx, \quad S_{ij}^K = \int_{C_K} \Phi_j^K \left(\Phi_i^K\right)' dx.$$

This is an ordinary differential system which solution is denoted $\mathbf{f} = (\mathbf{f}^K)_{1\le K\le N}$ with $\mathbf{f}^K = (f_0^K,\dots,f_k^K)$:

$$M^K \partial_t \mathbf{f}^K(t,v) + S^K \mathbf{f}^K(t,v) = F(\mathbf{f},t,v), \quad 1 \le K \le N. \tag{4.5}$$

We denote $f^{n+1}(x,v) = Z(\Delta t,v) f^n(x,v)$ the obtained numerical scheme.

It is well-known that DG schemes may oscillate when sharp discontinuities are present in the solution. Hence in order to control these instabilities we consider generalized slope limiters [23]. We first define the interface fluxes as

$$u^-_{K+\frac{1}{2}} = \bar{f}^K - m\left(\bar{f}^K - f^K(x_{K+\frac{1}{2}}), \bar{f}^K - \bar{f}^{K-1}, \bar{f}^{K+1} - \bar{f}^K\right) \tag{4.6}$$

$$u^+_{K-\frac{1}{2}} = \bar{f}^K + m\left(\bar{f}^K - f^K(x_{K-\frac{1}{2}}), \bar{f}^K - \bar{f}^{K-1}, \bar{f}^{K+1} - \bar{f}^K\right) \tag{4.7}$$

where $\bar{f}^K$ is the average of f^K on C_K and where m is the minmod function limiter

$$m(a_1,a_2,a_3) = \begin{cases} s\cdot \min_j |a_j| & \text{if } s = \text{sign}(a_1) = \text{sign}(a_2) = \text{sign}(a_3) \\ 0 & \text{otherwise} \end{cases}$$

Then the generalized slope limiter technique consists in replacing f^K on each cell C_K with $\Lambda\Pi_h$ defined by

$$\Lambda\Pi_h(f^K) = \begin{cases} f^K & \text{if } u^+_{K-\frac{1}{2}} = f^K(x_{K-\frac{1}{2}}) \text{ and } u^+_{K+\frac{1}{2}} = f^K(x_{K+\frac{1}{2}}), \\ \bar{f}^K + (x-x_K)m(f^K_x, \dfrac{\bar{f}^{K+1}-\bar{f}^K}{\Delta x/2}, \dfrac{\bar{f}^K-\bar{f}^{K-1}}{\Delta x/2}) & \text{otherwise.} \end{cases}$$

4.2. A DG scheme for the bitemperature Euler system In this section we approximate the initial value problem for system (2.12). An initial data $\mathcal{U}(\cdot,0) = \mathcal{U}_0$ being given, we first define $\mathcal{U}^0 = \sum_{K=1}^N \mathcal{U}^{K,0}$ by setting, for $K = 1,\dots,N$:

$$\mathcal{U}^{K,0}(x) = \sum_{j=0}^k \mathcal{U}^{K,0}_j \Phi^K_j(x) \quad \text{with} \quad \mathcal{U}^{K,0}_j = \mathcal{U}_0(x^K_j), \quad j = 0,\dots,k.$$

Suppose that for $n \geq 0$, we have $\mathcal{U}^n(x) = \sum_{K=1}^N \sum_{j=0}^k \mathcal{U}^{K,n}_j \Phi^K_j(x)$. For $\alpha = e,i$, we define

$$U^n_\alpha = (\rho^n_\alpha, \rho^n_\alpha u^n, \mathcal{E}^n_\alpha) \quad \text{with} \quad \rho^n_\alpha = \rho^n c_\alpha. \tag{4.8}$$

Then $U^n_\alpha(x) = \sum_{K=1}^N \sum_{j=0}^k U^{K,n}_{\alpha,j} \Phi^K_j(x)$ with

$$U^{K,n}_{\alpha,j} = (c_\alpha \rho^{K,n}_j, c_\alpha \rho^{K,n}_j u^{K,n}_j, \mathcal{E}^{K,n}_{\alpha,j}).$$

Our numerical scheme is based on system (3.5) where the two-velocity discrete BGK model described in Example 2, subsection 3.1.2 is used for both ions and electrons.

Step 1: projection onto equilibrium
In this step, we define f^n_α for $\alpha = e,i$ as

$$f^n_\alpha(x,\xi) = \sum_{K=1}^N \sum_{j=0}^k M_\alpha(U^{K,n}_{\alpha,j}, \xi) \Phi^K_j(x), \quad \xi = 1,2 \tag{4.9}$$

that is, on each cell C_K, the Lagrange interpolate of $M_\alpha(U^n_\alpha(x),\xi)$ on C_K.

REMARK 4.1. *Define* $U(x,t)=\int_X P(\xi)(f(x,t,\xi))d\xi$. *By linearity if*

$$f(x,t,v)=\sum_{K=1}^{N}\sum_{j=0}^{k} f_j^K(t,v)\Phi_j^K(x)$$

then

$$U(x,t)=\sum_{K=1}^{N}\sum_{j=0}^{k} U_j^K(t)\Phi_j^K(x) \quad \text{with} \quad U_j^K(t)=\int_X P(\xi)(f_j^K(t,\xi))d\xi.$$

In particular, the compatibility conditions (3.2) *imply that* $U_\alpha^n(x)=\int_X P(\xi)(f_\alpha^n(x,\xi))d\xi$.

Step 2: transport by DG method. For $\alpha\in\{e,i\}$ and $\xi\in\{1,2\}$ we solve the transport equations

$$\begin{cases}\partial_t f_\alpha + a(\xi)\partial_x f_\alpha = 0, & t\in[t_n,t_{n+1}],\\ f_\alpha(x,t_n)=f_\alpha^n(x).\end{cases}$$

We choose the same $a(\xi)$ for ions and electrons by using the subcharacteristic condition. Here f_α takes values in $\mathbb{R}^3$ and the procedure described in the Preliminary section is applied to all its components and for each $\xi\in\{1,2\}$, hence 6 times. We still use the notation $Z(\Delta t,\xi)$ for the solution:

$$f_\alpha^{n+\frac{1}{2}}(\xi)=Z(\Delta t,\xi)f_\alpha^n(\xi)$$

and we denote

$$f_\alpha^{n+\frac{1}{2}}=Z^{\Delta t}f_\alpha^n.$$

Here a (k+1)-SSP-Runge-Kutta method is used for the time integration. According to remark 4.1 we then define

$$U_\alpha^{n+\frac{1}{2}}(x)=\int_X P(\xi)(f_\alpha^{n+\frac{1}{2}}(x,\xi))d\xi=\sum_{K=1}^{N}\sum_{j=0}^{k} U_{\alpha,j}^{K,n+\frac{1}{2}}\Phi_j^K(x)$$

with

$$U_{\alpha,j}^{K,n+\frac{1}{2}}=\int_X P(\xi)(f_{\alpha,j}^{K,n+\frac{1}{2}}(\xi))d\xi. \tag{4.10}$$

For the first component of f_α we have by (3.4)

$$f_{\alpha,1}^n(1)=c_\alpha\frac{\lambda_2\rho^n-\rho^n u^n}{\lambda_2-\lambda_1}, \quad f_{\alpha,1}^n(2)=c_\alpha\frac{-\lambda_1\rho^n+\rho^n u^n}{\lambda_2-\lambda_1}.$$

Solving the related transport equations preserve this property: $f_{\alpha,1}^{n+\frac{1}{2}}=c_\alpha f_1^{n+\frac{1}{2}}$ where $f_1^{n+\frac{1}{2}}$ is the solution with data $f_{\alpha,1}^n/c_\alpha$. Consequently for $\alpha\in\{e,i\}$ $\rho_\alpha^{n+\frac{1}{2}}=c_\alpha\rho^{n+\frac{1}{2}}$ where $\rho^{n+\frac{1}{2}}=\rho_e^{n+\frac{1}{2}}+\rho_i^{n+\frac{1}{2}}$.

Step 3: force and source terms. For $\alpha = e,i$

$$f_\alpha^{n+\frac{3}{4}} = f_\alpha^{n+\frac{1}{2}} - \Delta t \frac{q_\alpha}{m_\alpha} E^{n+1} \mathcal{N} f_\alpha^{n+\frac{3}{4}} + \Delta t B_{\alpha\beta}(f_e^{n+\frac{3}{4}}, f_i^{n+\frac{3}{4}}), \quad \beta \neq \alpha$$

and

$$U_\alpha^{n+1} = \int_X P(\xi)(f_\alpha^{n+\frac{3}{4}}(\xi))d\xi = (\rho_\alpha^{n+1}, \rho_\alpha^{n+1} u_\alpha^{n+1}, \mathcal{E}_\alpha^{n+1}).$$

We obtain

$$U_\alpha^{n+1} = U_\alpha^{n+\frac{1}{2}} - \Delta t \frac{q_\alpha}{m_\alpha} E^{n+1} \mathcal{N} U_\alpha^{n+1} + S(T_e^{n+1}, T_i^{n+1}).$$

This expression is not implemented in the code. It is an intermediate result which is taken into account in Step 4. In particular $f_{\alpha,1}^{n+\frac{3}{4}} = f_{\alpha,1}^{n+\frac{1}{2}}$, so

$$\rho_\alpha^{n+1} = \rho_\alpha^{n+\frac{1}{2}} = c_\alpha \rho^{n+1}, \quad \rho^{n+1} = \rho_e^{n+1} + \rho_i^{n+1}. \tag{4.11}$$

Step 4: coupling with Maxwell-Ampère and Poisson equations.

$$\begin{cases} \dfrac{q_e}{m_e}\rho_e^{n+1} + \dfrac{q_i}{m_i}\rho_i^{n+1} = 0, \\ \dfrac{q_e}{m_e}\rho_e^{n+1} u_e^{n+1} + \dfrac{q_i}{m_i}\rho_i^{n+1} u_i^{n+1} = 0. \end{cases}$$

Hence $u_i^{n+1} = u_e^{n+1}$. We set $u^{n+1} = u_i^{n+1} = u_e^{n+1}$. As $q_e = -e$ and $q_i = Ze$, we get as in the continuous case $\rho_e^{n+1} = c_e \rho^{n+1}$, $\rho_i^{n+1} = c_i \rho^{n+1}$, which is consistent with (4.11). We have analogously to (3.7)

$$\begin{cases} \rho_\alpha^{n+1} = \rho_\alpha^{n+\frac{1}{2}}, & \alpha = e,i, \\ \rho_e^{n+1} u^{n+1} = \rho_e^{n+\frac{1}{2}} u_e^{n+\frac{1}{2}} + \Delta t \dfrac{q_e}{m_e} E^{n+1} \rho_e^{n+1}, \\ \rho_i^{n+1} u^{n+1} = \rho_i^{n+\frac{1}{2}} u_i^{n+\frac{1}{2}} + \Delta t \dfrac{q_i}{m_i} E^{n+1} \rho_i^{n+1}, \\ \mathcal{E}_e^{n+1} = \mathcal{E}_e^{n+\frac{1}{2}} + \Delta t \dfrac{q_e}{m_e} E^{n+1} \rho_e^{n+1} u^{n+1} + \Delta t \nu_{ei}(T_i^{n+1} - T_e^{n+1}), \\ \mathcal{E}_i^{n+1} = \mathcal{E}_i^{n+\frac{1}{2}} + \Delta t \dfrac{q_i}{m_i} E^{n+1} \rho_i^{n+1} u^{n+1} - \Delta t \nu_{ei}(T_i^{n+1} - T_e^{n+1}). \end{cases} \tag{4.12}$$

The equations on mass and momentum give ρ^{n+1} and u^{n+1}:

$$\begin{cases} \rho^{n+1} = \rho^{n+\frac{1}{2}}, \\ \rho^{n+1} u^{n+1} = \rho_e^{n+\frac{1}{2}} u_e^{n+\frac{1}{2}} + \rho_i^{n+\frac{1}{2}} u_i^{n+\frac{1}{2}}. \end{cases} \tag{4.13}$$

We then compute E^{n+1} as in the continuous case ([5]):

$$c_e \rho^{n+1} u^{n+1} = \rho_e^{n+\frac{1}{2}} u_e^{n+\frac{1}{2}} + \Delta t \frac{q_e}{m_e} E^{n+1} \rho^{n+1} c_e,$$
$$c_i \rho^{n+1} u^{n+1} = \rho_i^{n+\frac{1}{2}} u_i^{n+\frac{1}{2}} + \Delta t \frac{q_i}{m_i} E^{n+1} \rho^{n+1} c_i,$$

hence

$$\Delta t \frac{q_e}{m_e} E^{n+1} \rho_e^{n+1} = -\Delta t \frac{q_i}{m_i} E^{n+1} \rho_i^{n+1} = -c_i \rho_e^{n+\frac{1}{2}} u_e^{n+\frac{1}{2}} + c_e \rho_i^{n+\frac{1}{2}} u_i^{n+\frac{1}{2}} \tag{4.14}$$

and

$$\begin{cases} \mathcal{E}_e^{n+1} = \mathcal{E}_e^{n+\frac{1}{2}} + u^{n+1} \left(-c_i \rho_e^{n+\frac{1}{2}} u_e^{n+\frac{1}{2}} + c_e \rho_i^{n+\frac{1}{2}} u_i^{n+\frac{1}{2}} \right) + \Delta t \nu_{ei} (T_i^{n+1} - T_e^{n+1}) \\ \mathcal{E}_i^{n+1} = \mathcal{E}_i^{n+\frac{1}{2}} + u^{n+1} \left(c_i \rho_e^{n+\frac{1}{2}} u_e^{n+\frac{1}{2}} - c_e \rho_i^{n+\frac{1}{2}} u_i^{n+\frac{1}{2}} \right) + \Delta t \nu_{ei} (T_e^{n+1} - T_i^{n+1}). \end{cases} \tag{4.15}$$

As

$$T_\alpha^{n+1} = \left(\frac{\mathcal{E}_\alpha^{n+1}}{\rho_\alpha^{n+1}} - \frac{1}{2} (u^{n+1})^2 \right) \frac{(\gamma_\alpha - 1) m_\alpha}{k_B}$$

system (4.15) can be solved explicitly at each Lagrange point. Finally we obtain $\mathcal{U}^{n+1}(x)$, an approximation of $\mathcal{U}(x, t_{n+1})$.

Remark 4.2. *Formula (4.14) corresponds to an approximation of the genaralized Ohm's Law.*

Remark 4.3. *Note that the definition of U_α^{n+1} is consistent with (4.8).*

We summarize the time step: $\mathcal{U}^n$ being known by its values at each Lagrange point of each cell, we compute the following quantities at the same Lagrange points:

1. U_e^n and U_i^n by (4.8)
2. f_e^n and f_i^n by (4.9)
3. DG algorithm to obtain $f_e^{n+\frac{1}{2}}$ and $f_i^{n+\frac{1}{2}}$
4. $\rho_\alpha^{n+\frac{1}{2}} = \int_X P(\xi) f_{\alpha,1}^{n+\frac{1}{2}}(\xi) d\xi$ and $\rho_\alpha^{n+\frac{1}{2}} u_\alpha^{n+\frac{1}{2}} = \int_X P(\xi) f_{\alpha,2}^{n+\frac{1}{2}}(\xi) d\xi$ for $\alpha \in \{e, i\}$
5. $\rho^{n+1} = \sum_{\alpha=e,i} \rho_\alpha^{n+\frac{1}{2}}$, $\rho^{n+1} u^{n+1} = \sum_{\alpha=e,i} \rho_\alpha^{n+\frac{1}{2}} u_\alpha^{n+\frac{1}{2}}$
6. $\mathcal{E}_e$ and $\mathcal{E}_i$ by (4.15)

4.3. Focus on the time discretization The scheme described in subsection 4.2 can be viewed as a fractional step method which computes the approximate solution $\mathcal{U}_h^{n+1}$ at time t_{n+1} as a function of $\mathcal{U}_h^n$:

$$\mathcal{U}^{n+1} = \mathbf{E}_{\Delta t}(\mathcal{U}^n). \tag{4.16}$$

This method is only first order in time, even if each step is high order, basically because in the underlying Trotter formula, when two operators A and B do not commute, $\exp(\Delta t(A+B)) = \exp(\Delta t A)\exp(\Delta t B) + O(\Delta t^2)$. We can view this procedure as an explicit RK1 Euler scheme applied to the semi-discretized system obtained by performing the DG spacial discretization of system (2.5):

$$\partial_t \mathcal{U}_h = \mathbf{G}(\mathcal{U}_h).$$

It is important to increase the order in time when one increases the order in space, otherwise you will not observe any significant improvement of the numerical results, see section 5 below. For this purpose, we use higher order N_r steps explicit Runge Kutta schemes. The approximate solution $\mathcal{U}_h^n$ being known, we set

$$Y_1 = \mathcal{U}_h^n, \quad V_1 = Y_1, \quad \begin{cases} Y_{i+1} = \mathbf{E}_{\Delta t}(V_i), \\ V_{i+1} = d_{i1}^{(N_r)} \mathcal{U}_h^n + d_{i2}^{(N_r)} Y_{i+1}, \end{cases} \quad i = 1, \ldots, N_r, \tag{4.17}$$

and

$$\mathcal{U}_h^{n+1} = V_{N_r+1}. \tag{4.18}$$

The scheme is defined by a $N_r \times 2$ matrix $D^{(N_r)} = \left(d_{ij}^{(N_r)}\right)$. Here we set:

$$D^{(1)} = (0,1), \quad D^{(2)} = \begin{pmatrix} 0 & 1 \\ \frac{1}{2} & \frac{1}{2} \end{pmatrix}, \quad D^{(3)} = \begin{pmatrix} 0 & 1 \\ \frac{3}{4} & \frac{1}{4} \\ \frac{1}{3} & \frac{2}{3} \end{pmatrix}.$$

The case $N_r = 1$ is the explicit Euler method. It is used with a P^0-DG discretization. The case $N_r = 2$ is the RK2 Heun method, used with a P^1-DG discretization. This method is Strong Stability Preserving (SSP) [24]. For the third-order $N_r = 3$, we consider the Shu-Osher RK3-SSP scheme [23], used with P^2-DG discretization. It is to be noted that the case $N_r = 2$ can also be viewed as a DeC method [1].

We consider here the following CFL condition:

$$CFL = \frac{\Delta t}{\Delta x}|v| \leq \frac{1}{2k+1} \tag{4.19}$$

where k is the degree of the polynomial [18].

5. Numerical results This section is devoted to the numerical validation of the numerical scheme that is constructed in the previous section. The numerical method is firstly applied to the compressible Euler system (2.8) and next to the bitemperature Euler system (2.5).

5.1. Compressible Euler system

5.1.1. Euler isentropic In this subsection we test the the efficiency of the high order in time of the method and we show the convergence in space of the scheme for Euler equations (2.8) by considering the case of isentropic flow i.e when $\gamma = 3$ and $p = \rho^\gamma$, with the initial conditions

$$\begin{pmatrix} \rho_0 \\ u_0 \\ p_0 \end{pmatrix} = \begin{pmatrix} 1 + 0.5\sin(\pi x) \\ 0 \\ \rho_0^\gamma \end{pmatrix}$$

where the domain is $\Omega = [-1,1]$, the final time $T = 0.1$ and we take $CFL = 0.1$. We plot in Figure 5.1 the numerical order of convergence of the method. The considered error is the L^2-norm. We observe that we get $k+1$ order when we choose for a P^k-DG discretisation the space with a time discretisation of order $k+1$. We also give in table 5.1 the numerical rate of convergence. We have measured the L^2-error

$$E^N = \|u_h(T,\cdot) - \hat{u}_e(T,\cdot)\|,$$

k	N	E^N	Order α_N
0	5	0.0902	-
	10	0.0485	0.8983
	20	0.0247	0.9735
	40	0.0125	0.9826
	80	0.0063	0.9885
1	5	0.1214	-
	10	0.0193	2.6533
	20	0.0042	2.2056
	40	0.0010	2.0377
	80	$2.5414.10^{-4}$	2.0034
2	5	0.0286	-
	10	0.0059	2.2883
	20	$7.1844.10^{-4}$	3.0267
	40	$1.1757.10^{-4}$	2.6114
	80	$1.7051.10^{-5}$	2.7856

TABLE 5.1. *Error and numerical rate of convergence of u for Euler equations for $k=0,1,2$. N denotes the number of elements.*

where $\hat{u}_e$ is the numerical solution which has been computed using a very fine grid and the approximation rate of convergence

$$\alpha_N = \left(\frac{1}{\log 2}\right)\left(\log E^{2N} - \log E^N\right).$$

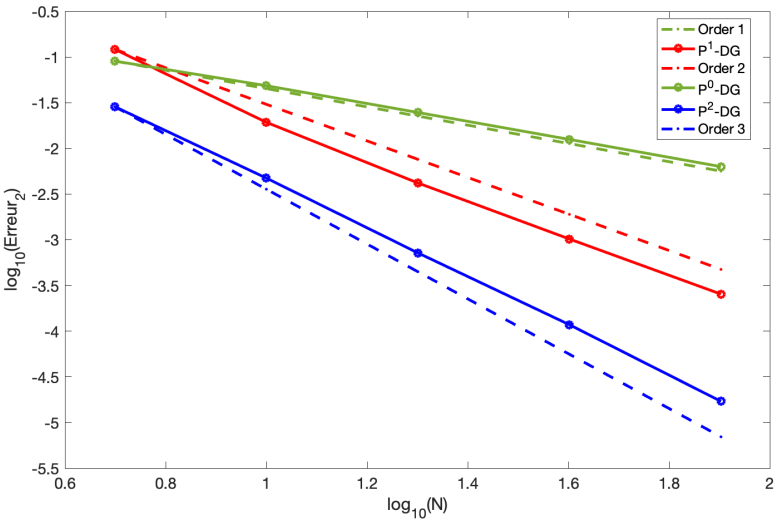

FIG. 5.1. *Convergence of u for Euler equations*

We next show in Figure 5.2 the impact of the high order Runge-Kutta method associated to the high order DG-space discretization. As expected we obtain the optimal order two in space when we use the P^1-DG space discretization associated to a second-order Runge-Kutta (RK2) method as opposed to the Euler method for the time discretization.

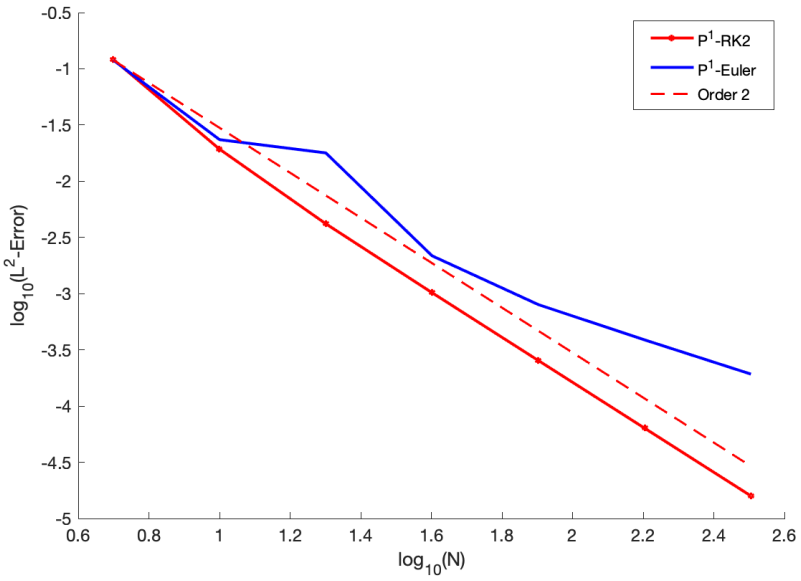

FIG. 5.2. *Convergence of u of Euler equations for P^1-DG space discretization with RK2 (red) and Euler (blue) time discretization.*

5.1.2. Shu-Osher test case We consider the test case [29] applied to the compressible Euler system for $\gamma = 1.4$. The initial conditions of the Shu-Osher test are given by

$$\begin{pmatrix}\rho_0\\ u_0\\ p_0\end{pmatrix} = \begin{pmatrix}3.857143\\ 2.6929369\\ 10.333333\end{pmatrix} \text{ if } x\in[-5,-4],\quad \begin{pmatrix}\rho_0\\ u_0\\ p_0\end{pmatrix} = \begin{pmatrix}1+0.2\sin(5x)\\ 0\\ 1\end{pmatrix} \text{ if } x\in[-4,5],$$

on the domain $[-5,5]$ and the final time of the problem is $T = 1.8$.

The reference solution represented in Figure 5.3 is obtained with the P^2-DG method with 5000 points. We compare in Figure 5.3 the results obtained with P^0, P^1 and P^2 method for 512 points with the reference solution. We observe that the oscillations are well captured by the P^2 reconstruction and that the precision increases with the order of the scheme.

5.1.3. Blast waves In order to highlight the advantages for using a high order method, we consider the test case proposed by Collela and Woodward [16] devoted to the compressible Euler system for $\gamma = 1.4$. We consider the initial conditions $\rho_0 = 1,\ u_0 = 0,\ p_0 = 10^3 1_{[0,0.1[} + 10^{-2} 1_{[0.1,0.9[} + 10^2 1_{[0.9,1]}$. The density and the energy are displayed in Figure 5.4 for 1000 points in space. As observed in Figure 5.4, the P^2 reconstruction is able to catch correctly the second pick.

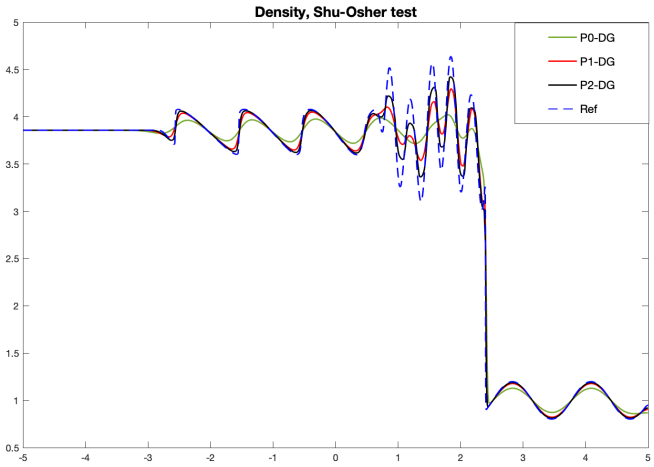

FIG. 5.3. *Density for the Shu-Osher test case.*

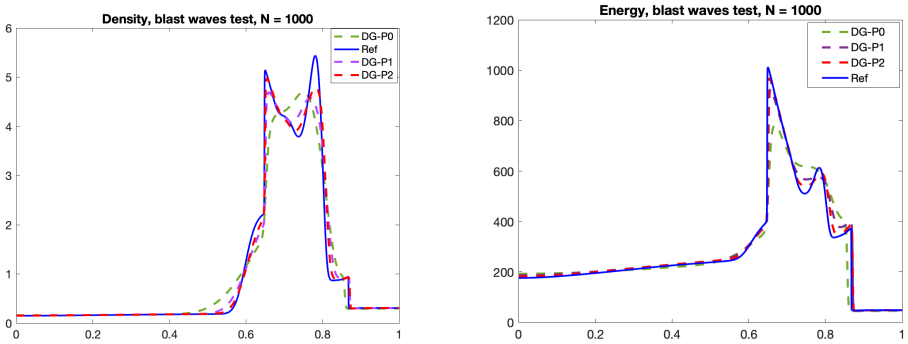

FIG. 5.4. *Density (left) and Energy (right) for the blast waves.*

All the previous numerical tests have been tested in [4] for a RD scheme and analogous results are obtained.

5.2. Bitemperature Euler system Next the numerical method is applied to the bitemperature Euler system (2.12). In subsection 5.2.1, we perform a convergence study for the DG kinetic scheme for the P^1 and the P^2 reconstruction. In the next test cases, the DG kinetic scheme for the P^2 reconstruction is compared with the kinetic scheme for a finite volume space discretization (FV kinetic scheme) and the Suliciu method developed in [5].

5.2.1. Analytical test case We look for a smooth analytical solution of system (2.12). We assume that ρ and u are constant, so that the system reduces to

$$\begin{cases} \partial_x(ZT_e+T_i)=0, \\ \partial_t T_e+u\partial_x T_e=\beta_e(T_i-T_e), \\ \partial_t T_i+u\partial_x T_i=\beta_i(T_e-T_i) \end{cases} \tag{5.1}$$

with

$$\beta_\alpha=\frac{\nu_{ei}m_\alpha(\gamma_\alpha-1)}{\rho c_\alpha k_B}, \quad \alpha\in\{e,i\}.$$

We choose initial temperatures $T_e(x,0)=T_{e,0}(x)$, $T_i(x,0)=T_{i,0}(x)$ such that

$$\partial_x(ZT_{e,0}+T_{i,0})=0. \tag{5.2}$$

It is easy to compute the solution (T_e,T_i) of the last two equations: denoting $\beta_1+\beta_2=\beta$, $\mu=\frac{\gamma_e-1}{Z}+\gamma_i-1$:

$$\begin{aligned} T_e(x+ut,t)&=\frac{1}{\mu}\left(\frac{\gamma_e-1}{Z}(T_{e,0}(x)-T_{i,0}(x))\mathrm{e}^{-\beta t}+(\gamma_i-1)T_{e,0}(x)+\frac{\gamma_e-1}{Z}T_{i,0}(x)\right) \\ T_i(x+ut,t)&=\frac{1}{\mu}\left((\gamma_i-1)(T_{i,0}(x)-T_{e,0}(x))\mathrm{e}^{-\beta t}+(\gamma_i-1)T_{e,0}(x)+\frac{\gamma_e-1}{Z}T_{i,0}(x)\right) \end{aligned} \tag{5.3}$$

Then one can observe that if $\gamma_e\neq\gamma_i$ the first equation of (5.1) cannot be satisfied unless $\partial_x T_{e,0}=\partial_x T_{i,0}=0$. Therefore we set $\gamma_e=\gamma_i$. In that case, if (5.2) is satisfied then we have a solution of the bitemperature Euler system.

We choose $\nu_{ei}=1$, $T=0.1$, $\Omega=[0,1]$ and $CFL=0.1$. We plot in Figure 5.5 the convergence of the method for the bitemperature Euler system (2.12). In contrast to compressible Euler system, the numerical simulation show a convergence of order k when using a P^k-DG for the space discretisation and with a $(k+1)$-RK time approximation. We also give in table 5.2 the numerical rate of convergence. For the electronic temperature, we have measured the L^2-error

$$E_{te}^N=||T_e(T,\cdot)-\hat{T}_e(T,\cdot)||,$$

where $\hat{T}_e$ is the exact solution given in (5.3) and the approximation rate of convergence is computed as

$$\alpha_N^t=\left(\frac{1}{\log 2}\right)\left(\log E_{te}^{2N}-\log E_{te}^N\right).$$

5.2.2. Double shock In this test case, we consider the following physical parameters:

$$\begin{aligned} k_B=1.3807\times10^{-23}\ \mathrm{J.K^{-1}}, \quad m_e=9,1094\times10^{-31}\ \mathrm{kg}, \quad m_i=1.6726\times10^{-27}\ \mathrm{kg}, \\ e=-q_e=q_i=1.6022\times10^{-19}\ \mathrm{C}, \quad \gamma_e=\frac{5}{3}, \quad \gamma_i=\frac{7}{5}. \end{aligned}$$

We consider a double shock for $\nu_{ei}=0$ which is a Riemann problem

$$\rho_L=1, \quad u_L=10^5, \quad T_{e,L}=2.310^7, \quad T_{i,L}=2.310^6$$

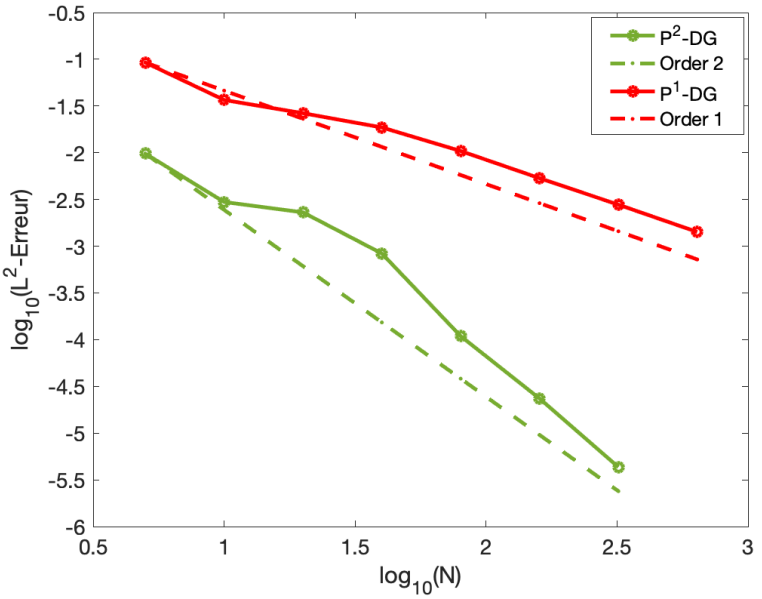

FIG. 5.5. *Convergence of electronic temperature for the bitemperature Euler system*

k	N	E_{te}^N	Order α_N
1	5	0.0924	-
	10	0.0265	1.8023
	20	0.0186	0.5061
	40	0.0104	0.8380
	80	0.0053	0.9663
	160	0.0028	0.9414
	320	0.0014	0.9698
2	5	0.0099	-
	10	0.0030	1.7203
	20	0.0023	0.3681
	40	$8.3520e^{-4}$	1.4621
	80	$1.089e^{-4}$	2.9380
	160	$2.3431e^{-5}$	2.2176
	320	$4.323e^{-6}$	2.4281

TABLE 5.2. *Error and numerical rate of convergence of electronic temperature for the bitemperature Euler system for $k=1,2$. N denotes the number of elements.*

$$\rho_R = 1, \quad u_R = -10^5, \quad T_{e,R} = 2.3\,10^7, \quad T_{i,R} = 2.3\,10^6.$$

The results for electronic and ionic temperatures are displayed in Figures 5.6 and 5.7 at time $t = 4.09\,10^{-7}$ s for 10000 points in space. They are obtained with the Suliciu method, the finite volume kinetic method constructed in [5] and the DG method with a P^2 reconstruction developed in this paper. The three methods show analogous results.

5.2.3. Double rarefaction wave

Using similar physical parameters as in subsection 5.2.2 we consider here a rarefaction wave for $\nu_{ei}=0$ which is a Rieman problem

$$\begin{aligned}&\rho_L=1, \quad u_L=-10^5, \quad T_{e,L}=2.310^7, \quad T_{i,L}=2.310^6,\\ &\rho_R=1, \quad u_R=10^5, \quad T_{e,R}=2.310^7, \quad T_{i,R}=2.310^6.\end{aligned}$$

We take $\gamma_e=5/3$ and $\gamma_i=7/5$. This test case is a rarefaction wave computed at time $t=4.0910^{-7}$ s for 10000 points in space. In this test case, an analytical solution can be computed. The results displayed in Figure 5.8 and in Figure 5.9 compare for electronic and ionic temperatures the P^2 reconstruction with the finite volume kinetic scheme and the Suliciu scheme developed in [5]. All the scheme show a good agreement with the exact solution.

5.2.4. Stationary shock We consider here the test case of the stationary shock presented in [5] in the case $\nu_{ei}=100$ and with the following parameters:

$$k_B=1.0, \quad m_e=10^{-3}, \quad m_i=1.0, \quad Z=1.0, \quad \gamma_e=\gamma_i=5/3 \tag{5.4}$$

In that case, the left and the right states of the Riemann problem are the following

$$\begin{aligned}&\rho_L=1.001, \quad u_L=10, \quad T_{e,L}=1, \quad T_{i,R}=1,\\ &\rho_R=3.640330609, \quad u_R=2.749750250, \quad T_{e,R}=3, \quad T_{i,R}=17.5060240977.\end{aligned}$$

The results displayed in Figure 5.10 and in Figure 5.11 are computed for 10000 points in space and at time $t=0.005s$.

5.2.5. Sod test case We finally consider the Sod test case with the parameters (5.4), $\nu_{ei}=0$, a final time $t=0.05\,s$ and

$$\begin{aligned}&\rho_L=1, \quad u_L=0, \quad T_{e,L}=1, \quad T_{i,R}=1,\\ &\rho_R=0.125, \quad u_R=0, \quad T_{e,R}=2, \quad T_{i,R}=3.\end{aligned}$$

Figures 5.13 and 5.12 represent ionic and electronic temperatures for 10000 points in space with Suliciu, kinetic and discontinuous Galerkin method with a P^2 reconstruction. The three schemes show the same results. In particular, the "plateaux" after the shocks have the same amplitude. The DG kinetic scheme shows some oscillations for the electronic temperatures. However, these oscillations do not propagate.

6. Conclusion and perspectives In this paper, we have developed a DG-kinetic scheme for the bitemperature Euler system for any order of space discretization. The principle is to consider a discrete BGK model as in [5] and to construct a DG discretisation with k-th degree basis for the space discretization and with an $(k+1)$-SSP-Runge-Kutta method for the time discretization. Due to the kinetic model, a special treatment has been used to implement the order in time. This method has been illustrated on several test cases and numerical order has been investigated on both conservative Euler equations and nonconservative bitemperature Euler model. It is to be noted that in the nonconservative case, when shocks occur, the electronic and ionic temperatures cannot be predicted analytically, even in the framework of a Riemann problem as for a conservative system. They can depend on the numerical viscosity. A crucial fact here is that even in the presence of shocks we observe that whatever the order, the DG method converges to the same solutions as the ones obtained in previous articles.

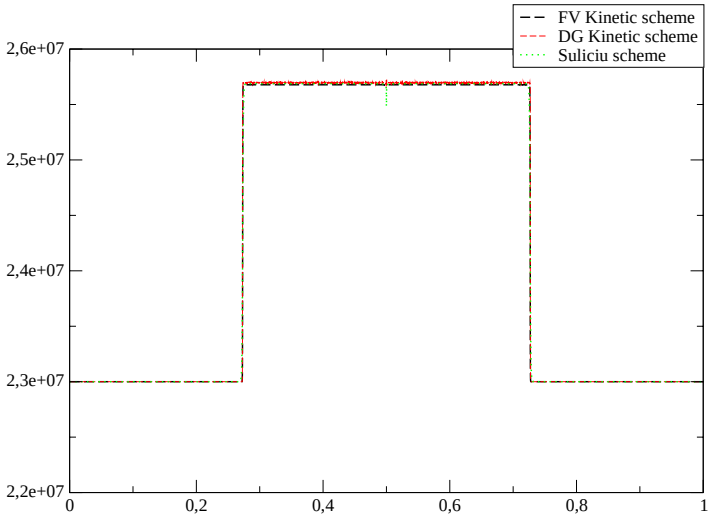

FIG. 5.6. *Electronic temperature for the double shock computed with the DG kinetic scheme, the finite volume kinetic scheme, the Suliciu scheme, with* 10000 *points in space*

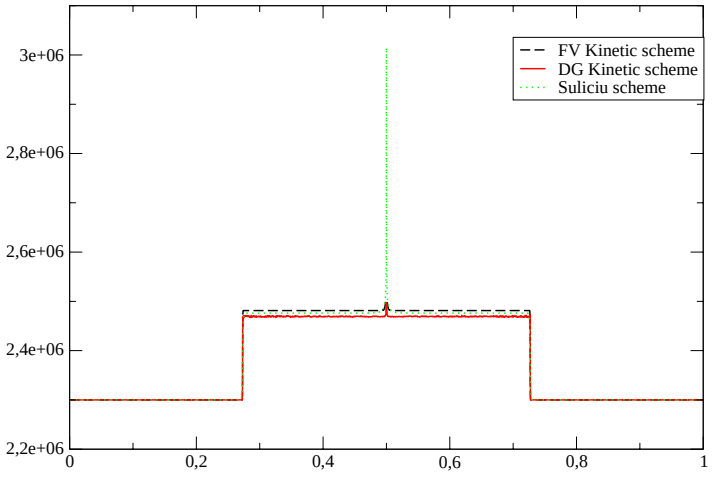

FIG. 5.7. *Ionic temperature for the double shock computed with the DG kinetic scheme for a* P^2 *reconstruction, the finite volume kinetic scheme, the Suliciu scheme, with* 10000 *points in space*

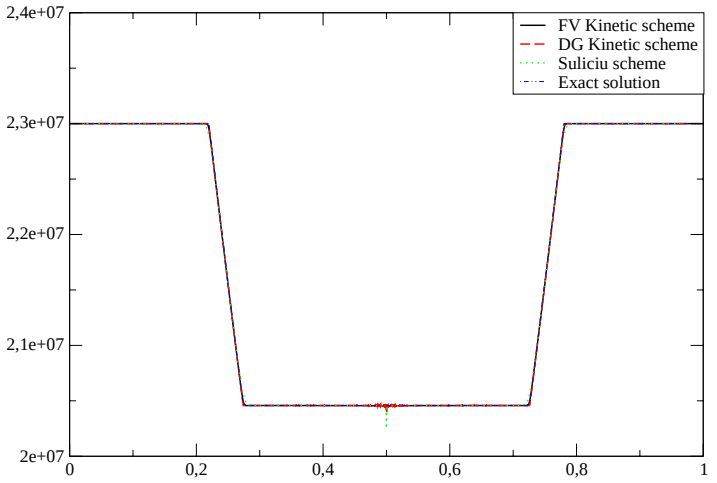

FIG. 5.8. *Electronic temperature for the double rarefaction wave computed with the DG scheme for a* P^2 *reconstruction, the kinetic scheme, the Suliciu scheme and the exact solution for* 10000 *points in space*

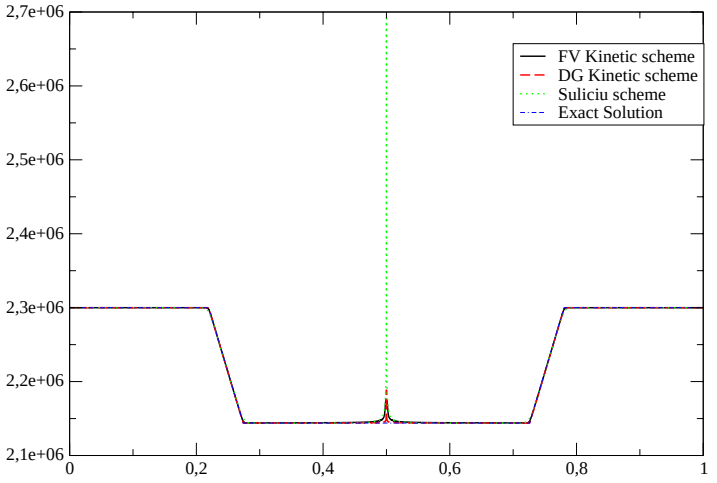

FIG. 5.9. *Ionic temperature for the double rarefaction computed with the DG kinetic scheme, the finite volume kinetic scheme, the Suliciu scheme and the exact solution for* 10000 *points in space*

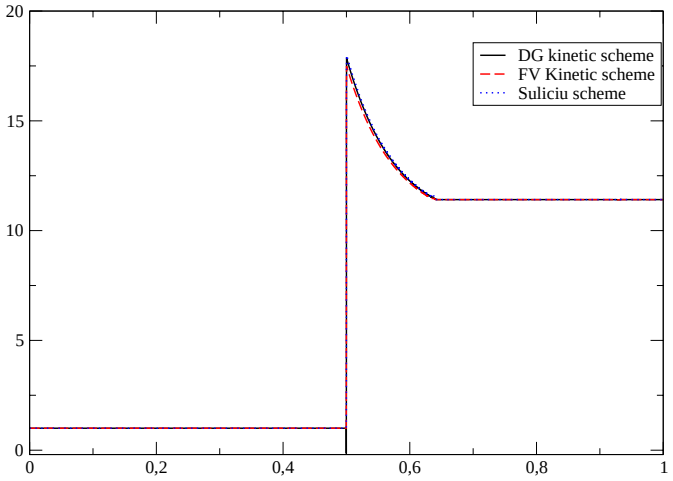

FIG. 5.10. *Ionic temperature for the stationary shock computed with the DG kinetic scheme, the finite volume kinetic scheme, the Suliciu scheme for* 10000 *points in space*

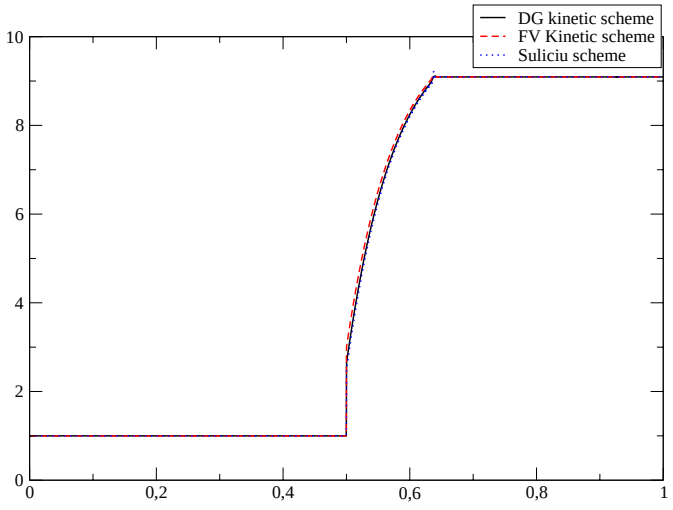

FIG. 5.11. *Electronic temperature for the stationary choc computed with the DG kinetic scheme, the finite volume kinetic scheme, the Suliciu scheme for* 10000 *points in space*

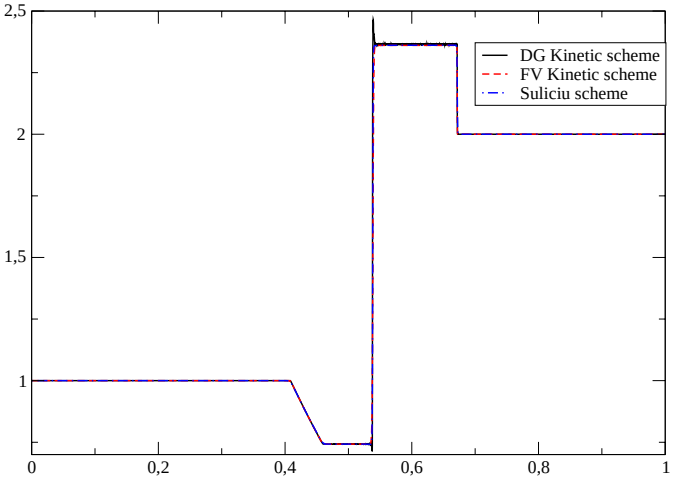

FIG. 5.12. *Electronic temperature for the sod test case computed with the DG kinetic scheme, the finite volume kinetic scheme, the Suliciu scheme computed with 10000 points.*

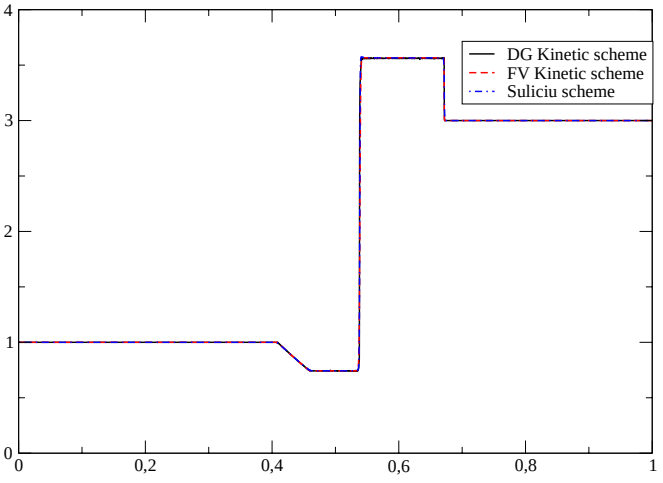

FIG. 5.13. *Ionic temperature for sod test case computed with the DG kinetic scheme, the finite volume kinetic scheme, the Suliciu scheme computed with* 10000 *points*

The generalization of the present work to a two dimensional framework as done in [10] for finite volumes is postponed to a future paper. Moreover in the present case, only the electric field has been taken into account. The question of the presence of the magnetic fields can also be considered as in [14] for a transverse magnetic field.

REFERENCES

[1] R. Abgrall High order schemes for hyperbolic problems using globally continous approximation and avoiding mass matrices *Journ. Sci. Comput.* 73, 461-494, (2017) 1, 4.3

[2] R. Abgrall, S. Karni, A comment on the computation of non-conservative products, *Journal of Computational Physics*, 229, 2759-2763, 2010, 1

[3] R. Abgrall, D. Torlo. Some preliminary results on high order asymptotic preserving computationally explicit kinetic scheme *Comm Maths Sci.*, 20, 297–326, 2022 1

[4] R. Abgrall, D. Torlo. High order preserving deferred correction implicit-explicit schemes for kinetic models. *Siam journal of scientific computing*, 42, 816–845, 2020 1, 5.1.3

[5] D. Aregba–Driollet, J. Breil, S. Brull, B. Dubroca, E. Estibals. Modelling and numerical approximation for the nonconservative bitemperature Euler model. *ESAIM: Mathematical Modelling and Numerical Analysis*, 52(4) (2018), 1353–1383, 2018 1, 2, 3, 3.1.1, 3.2, 3.2, 3.2, 3.2, 3.2, 4.2, 5.2, 5.2.2, 5.2.3, 5.2.4, 6

[6] D. Aregba-Driollet, S. Brull. About viscous approximations of the bitemperature euler system. *Communications in Math Sciences*, 17(4), 1135–1147, 2019 1

[7] D. Aregba-Driollet, S. Brull. Modelling and numerical study of the polyatomic bitemperature euler system. *Netw. Heterog. Media* 17, no. 4, 593–611, 2022 1

[8] D. Aregba-Driollet, S. Brull, X. Lhébrard. Nonconservative hyperbolic systems in fluid mechanics. In *SMAI 2017—8ème Biennale Française des Mathématiques Appliquées et Industrielles*, volume 64 of *ESAIM Proc. Surveys*. EDP Sci., 2018. 3

[9] D. Aregba-Driollet, S. Brull, Y.-J. Peng, Global existence of smooth solutions for a non-conservative bitemperature Euler model, *SIAM J. Math. Anal.* 53, no. 2, 1886-1907, 2021 1

[10] D. Aregba-Driollet, S. Brull, C. Prigent, A discrete velocity numerical scheme for the two-dimensional bitemperature Euler system, *SIAM J. Numer. Anal.* 60, no. 1, 28-51, 2022 1, 3, 6

[11] D. Aregba-Driollet, R. Natalini. Discrete kinetic schemes for multidimensional systems of conservation laws. *SIAM Journal on Numerical Analysis*, 37(6), 1973-2004, 2000 1, 3, 3.1.2, 3.2

[12] W. Boscheri, G. Dimarco High order modal Discontinuous Galerkin Implicit–Explicit Runge Kutta and Linear Multistep schemes for the Boltzmann model on general polygonal meshes *Computers and fluids*, 233, 2022 1

[13] F. Bouchut. Construction of BGK Models with a Family of Kinetic Entropies for a Given System of Conservation Laws. *Journal of Statistical Physics*, 95, 113-170, 1999 3.1, 3.1, 3.1.2

[14] S. Brull, B. Dubroca, X. Lhébrard Modelling and entropy satisfying relaxation scheme for the nonconservative bitemperature Euler system with transverse magnetic field, *Computers and Fluids*, 214, 2021. 1, 6

[15] S. Brull, B. Dubroca, C. Prigent. A kinetic approach of the bi-temperature Euler model, *Kinetic & Related Models*, 13 1, 33-61, 2020 1

[16] P. Collela, P.R. Woodward. The piecewse parabolic method (PPM) for gas dynamical simulations. *Journal of Computational Physics*, 54, 174-201, 1984 5.1.3

[17] C. Chalons, F. Coquel Navier-Stokes equations with several independant pressure laws and explicit predictor-corrector schemes *Numerische Math.* 103, 3, 451-478, 2005 1

[18] B. Cockburn, C.W. Shu, Runge–Kutta Discontinuous Galerkin Methods for Convection-Dominated Problems. *Journal of Scientific Computing* 16, 173–261, 2001 4.3

[19] D. Coulette, E. Franck, P. Helluy, M. Mehrenberger, L. Navoret, High-order implicit palindromic discontinuous Galerkin method for kinetic-relaxation approximation, *Computers & Fluids* 190, 2019. 1

[20] F. Coquel, C. Marmignon, Numerical methods for weakly ionized gas, *Astrophysics and Space Science*, 260, pp. 15–27, 1998 1

[21] G. Dal Maso, P. Le Floch, F. Murat, Definition and weak stability of nonconservative products, *Journal de mathématiques pures et appliquées*, 74, 483-548, 1995 1

[22] P. Gerhard, P. Helluy, V. Michel-Dansac Unconditionally stable and parallel Discontinuous Galerkin solver. *Computers and Mathematics with Applications*, 112, 116–137, 2022 1

[23] J. S. Hesthaven, T. Warburton, Nodal Discontinuous Galerkin Methods: Algorithms, Analysis, and Applications, *Springer Publishing Company, Incorporated* , 2007 4.1, 4.3

[24] L. Isherwood, Z. J. Grant, S. Gottlieb, Strong stability preserving integrating factor Runge-Kutta methods *SIAM J. Numer. Anal.* **56**, 3276–3307, 2018 4.3

[25] S. Jaiswal, A. Alexeenko, J. Hu, A discontinuous Galerkin fast spectral method for the full Boltzmann equation with general collision kernels *J Comput Phys*, **378**, 178–208, 2019 1

[26] S. Jaiswal, A. Alexeenko, J. Hu, A discontinuous Galerkin fast spectral method for the multi-species Boltzmann equation *Comput Methods Appl Mech Engrg*, 352, 56–84, 2019 1

[27] R. Natalini, A discrete kinetic approximation of entropy solutions to multidimensional scalar conservation laws. *J. Differential Equations* 148, no. 2, , 292–317, 1998 1

[28] C. Parés, Path-conservative numerical methods for nonconservative hyperbolic systems, *in Numerical methods for balance laws, vol. 24 of Quad. Mat., Dept. Math.*, Seconda Univ. Napoli, Caserta, 67–121, 2009 1

[29] C. W. Shu, S. Osher, Efficient implementation of essentially non-oscillatory shock-capturing schemes *Journal of Computational Physics*, Volume 77, Issue 2. 5.1.2

[30] A. Sangam, E. Estibals, Guillard, Derivation and numerical approximation of two-temperature Euler plasma model. *J. Comput. Phys.* 444, 2021 1

[31] Q. Wargnier, S. Faure, B. Graille, T. Magin, M. Massot, Numerical treatment of the nonconservative product in a multiscale fluid model for plasmas in thermal nonequilibrium: application to solar physics, *SIAM. J. Sci. Comput.*, 42, 1-27, 2020 1